Correlation between the atomic structure, formation energies, and optical absorption of neutral oxygen vacancies in amorphous silica

Sanghamitra Mukhopadhyay,* Peter V. Sushko, A. Marshall Stoneham, and Alexander L. Shluger†
Department of Physics & Astronomy, University College London, Gower Street, London WC1E 6BT, United Kingdom
(Received 30 December 2004; revised manuscript received 30 March 2005; published 13 June 2005)

We have calculated the distributions of structural parameters, formation energies, and defect levels of neutral oxygen vacancies (NOV) in amorphous silica (a-SiO_2). All oxygen sites in the amorphous structure were considered as possible candidates for vacancy formation in these calculations. The electronic structure of NOV configurations at 75 selected sites were studied using an embedded cluster method. The formation energies correlate with the Si—Si distance in relaxed vacancies and with vacancy relaxation energies. We carried out classical molecular dynamics calculations to test the possible effect of high temperature annealing on predictions from static calculations and found that it affects the high formation energy NOV configurations. Using classical atomistic simulations we then calculated the structure and formation energies of NOV in 220 different sites. For the 23 low formation energy NOV configurations obtained in classical calculations we calculated the optical absorption spectrum of NOV. We found that the $\sigma \rightarrow \sigma*$ transitions determine the low energy tail of the optical absorption spectrum and are strongly affected by the Si—Si distance in the vacancies. Therefore the red part of the NOV optical absorption spectrum should depend strongly on sample preparation and any further treatment which can create neutral oxygen vacancies. The results demonstrate how a statistical approach based on the embedded cluster method can be effectively applied to studying the properties of defects in amorphous materials.

DOI: 10.1103/PhysRevB.71.235204 PACS number(s): 61.72.Ji, 61.72.Bb, 71.55.Jv, 78.20.Bh

I. INTRODUCTION

The important role played by oxygen deficient centers (ODCs) in the optical and chemical properties of oxides is well appreciated and has been highlighted in several recent reviews.[1–4] In many cases the technologically important oxide is amorphous. However, most of the theoretical studies focus on crystalline materials and the additional complexity due to the structural disorder of the material is rarely taken into account directly. Recently, however, significant theoretical efforts have been invested in studying the structure and properties of oxygen deficient centers in amorphous silica,[5–8] a-SiO_2, which is one of the most important and extensively studied amorphous insulators.[9–11] The ODCs affect the performance of complementary metal-oxide-semiconductor based devices[1] and optical fibers[12] made of a-SiO_2, and therefore have been extensively studied experimentally[13–16] and have been classified into two types: ODC(I) and ODC(II).[14] However, our understanding of their structure and properties in a-SiO_2 still remains incomplete.

In this paper we will focus on ODC(I). This is diamagnetic and therefore has been studied only through its optical spectra and transformations into other defects. It gives rise to an optical absorption band with a maximum at around 7.6 eV in both crystalline quartz and in a-SiO_2.[14] There is a widely shared opinion that this absorption band can be attributed to neutral oxygen vacancy (NOV),[14,17,18] but this assignment is still being questioned.[19]

A large number of theoretical calculations based on the NOV model of ODC(I) as $O{\equiv}Si—Si{\equiv}O_3$ support the stability of this defect and several of them predict the optical excitation energy for the center with this structure to be close to 7.6 eV (see, for example, Refs. 20–22). However, almost no theoretical studies have focused on the effect of structural disorder in a-SiO_2 on the structure and properties of this defect. Various types of silica glass and thermal oxides (see, for example, Ref. 23) have different structures, densities, as well as defect and impurity contents. Moreover, the oxygen deficiency can be created by different means, e.g., during growth, deposition, cooling, annealing, and by irradiation. The experimental data suggest that properties of ODC(I), e.g., details of the optical absorption spectrum, do depend on the preparation conditions (see, for example, Refs. 17, 19, 24, and 25). Will NOV formed at different lattice sites reflect this dependence?

In this paper we assume the NOV model of ODC(I) and study the dependence of the structure and properties of this defect on the formation site in an amorphous sample. First, we assume that all oxygen sites are available for formation of NOV and obtain the distribution of vacancy formation energies and structural parameters. This approach provides the most complete distribution of properties, but which of the defect sites will really be occupied depends on the method of sample preparation and the mechanism of defect formation. In particular, close to thermodynamic equilibrium only oxygen sites with low NOV formation energies will accommodate NOV. We consider the structural properties of this subset of NOV and calculate their optical absorption spectrum. Using static calculations we find a strong correlation between the NOV formation energies and the Si—Si distances in relaxed vacancies. We also show that the NOV formation energies are correlated with the relaxation energies and with the displacements of the two Si atoms forming the Si—Si bond. We demonstrate that annealing of the vacancies using molecular dynamics induces a stronger short- and medium-range relaxation and results in generally lower formation en-

ergies and shorter Si—Si bonds. We also found that the energies of the $\sigma \rightarrow \sigma^*$ transitions are strongly correlated with the lengths of the Si—Si bonds and that the longer Si—Si bonds determine the red tail of the NOV optical absorption spectrum. We conclude that the red part of the NOV optical absorption spectrum should strongly depend on the details of sample preparation and further treatment which can form NOV. Our results predict densification of the amorphous samples in the presence of NOV. They demonstrate how a statistical approach based on the embedded cluster method can be effectively applied to studying the properties of defects in amorphous materials.

The paper is organized as follows. In the next section we describe the calculation techniques. The results of calculation are presented in Sec. III, and conclusions in Sec. IV.

II. CALCULATION TECHNIQUES

We used a combination of several techniques. First, the amorphous structure has been generated in periodic classical molecular dynamics (MD) calculations. Then an embedded cluster method[21,26,27] was applied to calculate properties of neutral oxygen vacancies at 75 representative oxygen sites in amorphous silica. These data were used to derive a set of interatomic potentials that described the interaction between atoms surrounding neutral oxygen vacancies in amorphous silica. Using these potentials we performed periodic classical static energy minimization calculations, where neutral oxygen vacancies at 220 oxygen sites were considered one at a time. Twenty configurations with the lowest vacancy formation energies and three configurations with higher formation energies were then selected and annealed using classical MD and their structural parameters were analyzed. Finally, we used the embedded cluster method to calculate the optical absorption spectrum of the 23 NOV selected in a-SiO_2.

A. Classical static and MD methods

To generate the amorphous structure we followed an earlier work by Vollmayr *et al.*[28] with several modifications summarized in Ref. 29. We used the DL_POLY code,[30] the Buckingham-type rigid-ion interatomic potentials developed by van Beest *et al.*[31] (BKS), and an NPT ensemble. The original BKS interatomic potentials have been modified[29] to improve their performance in MD simulations at high temperatures. The simulation cell, containing 648 atoms, was first heated to 7000 K at a rate of 5×10^{13} K/s (500 K per 10 ps), then equilibrated at 7000 K for 100 ps, and finally quenched to 0 K at a rate of 8×10^{12} K/s (50 K per 6 ps). The final configuration of the a-SiO_2 structure was further relaxed using a static energy minimization technique. The resulting a-SiO_2 model proves to be a continuous random network with all Si ions coordinated by four oxygen ions and all O ions coordinated by two silicon ions. It has a density of 2.37 g/cm^3, which is higher than the average density of 2.20 g/cm^3 usually attributed to amorphous silica.[32] This reflects the properties of the BKS potentials since the volume of the cubic simulation cell was not fixed during the MD calculations.

Static energy minimization calculations were carried out for the same amorphous SiO_2 structure as obtained in the MD simulations. First, the nondefective structure was considered. Then a single NOV was formed at an oxygen site and the total energy was minimized again. These calculations were repeated to accumulate statistics over 220 oxygen sites. They were carried out using the GULP[33] code and the classical shell model.[34] The original BKS interatomic potentials were modified to account for polarization of oxygen ions and to correctly reproduce the high-frequency dielectric constant of α-quartz.[21] The consistency of the rigid and shell model interatomic potentials has been tested in Ref. 29. The neutrality of the vacancies was preserved and the interactions between the lattice atoms in their vicinity were described by a specially fitted set of classical interatomic potentials discussed below (see Sec. III B). In all calculations both the internal coordinates and the unit cell vectors have been optimized keeping the shape of the cell orthorombic. To further anneal the vacancies, we used classical MD (see Sec. III B).

B. Embedded cluster method

The electronic structure of a-SiO_2 and that of defect centers was calculated using an embedded cluster technique implemented in the GUESS computer code.[21,26] The method combines an *ab initio* quantum-mechanical (QM) treatment of a defect and its surroundings, included into a QM cluster, with a classical description of the rest of the solid. It accounts for the electrostatic potential of the whole solid in the defect region and includes, consistently, both ionic and electronic contributions to the defect-induced polarization of the host lattice as well as the effect of the polarized lattice on the defect. The method and its applications to studying defects in α-quartz, a-SiO_2, and in other oxides have been thoroughly described in several recent publications.[21,26,27,29,35–37] Similar schemes have been reported in, for example, Refs. 38 and 39.

In the SiO_2 calculations, the QM cluster is terminated by Si^* atoms that are located at the Si sites of the SiO_2 structure and form an interface with the rest of the amorphous network which is treated classically. The Si^* atoms represent real Si atoms and their positions are optimized in the course of the total energy minimization. This is quite different from many molecular cluster schemes where a QM cluster is treated as a molecule terminated by artificial hydrogenlike pseudoatoms which are kept fixed in some positions determined by the Si—H or O—H distance in molecules.[20,40,41] The Si^* atoms are chosen so that they are coordinated by one quantum-mechanically treated oxygen and three classically treated oxygen ions. Their role is to represent the polar bond with the QM oxygen quantum-mechanically and reproduce the interaction with the three classical oxygens using classical interatomic potentials. The detailed description of Si^* atoms as applied to α-quartz and a-SiO_2 is given in Refs. 21, 27, and 29. Classical atoms are treated in the shell model and interact between themselves via the modified BKS interatomic potentials.[21,29] Other technical details are summarized below in Sec. III A.

The GUESS code[21,26] employed in this work plays the role

of a "master" program that calculates the total energy, total forces acting on all centers included in the calculation and performs geometry optimization of the whole system. The GAUSSIAN 98 package[42] is used for calculations of the quantum-mechanical contributions to the total energy and forces as well as for calculations of optical properties.

In the course of this extensive work we first performed the embedded cluster calculations of NOVs at 75 sites in the amorphous structure using the Hartree-Fock (HF) method and the computational scheme described in Refs. 29 and 35. However, the HF method does not allow us to reliably calculate the optical absorption energies due to its tendency to overestimate the band gap. Moreover, the original parametrization scheme[21] used for Si^* was designed to suit ground state calculations only. An improved embedding scheme, also used in this work, makes it possible to use density functional theory (DFT) for calculations of ground states and to employ the time-dependent DFT (TD-DFT) method for calculations of the optical transition energies. This scheme will be described in detail elsewhere.[43] We have checked that the original and the new parametrizations for the Si^* atoms give consistent sets of results for the ground state defect properties obtained using the HF method. The formation energies reported in this work were calculated using the HF approach. The new parametrization was employed to calculate the optical absorption spectrum of NOVs.

III. RESULTS OF CALCULATIONS

In this section we first discuss properties of isolated neutral oxygen vacancies formed at 75 lattice sites selected so that the structural parameters of these sites reflect the distribution of the structural parameters of the whole a-SiO_2 system.[29] Then the properties of a "low formation energy" subset are discussed. Finally, optical absorption spectra calculated for a selected subset of vacancies are presented.

A. Quantum-mechanical calculations

To characterize the properties of neutral oxygen vacancies we selected 75 oxygen sites (out of a total number of 432 for the 648-atom structure) so that the structural parameters of these sites span the distributions of Si—O bond lengths, Si—O—Si angles, and local topologies (ring structures). These distributions, calculated both for the whole structure and for the subset of 75 sites, are shown in Fig. 1. The distributions found for the selected oxygen sites are shown by shaded areas; they demonstrate that most combinations of Si—O distances and Si—O—Si angles have been taken into account. The same applies to the ring sizes.

The a-SiO_2 sample was modeled using a large spherical nanocluster centered at a selected vacancy site as described in Refs. 29 and 35. Approximately 700 atoms comprising a spherical region I at the center of the nanocluster are fully relaxed in the course of the energy minimization. The vacancy and its immediate surroundings were treated quantum-mechanically using $Si_2O_7Si_6^*$ QM clusters and the 6-31G basis set. In all cases the selected oxygen site was at the center of the cluster formed by two adjacent tetrahedra. Each cluster

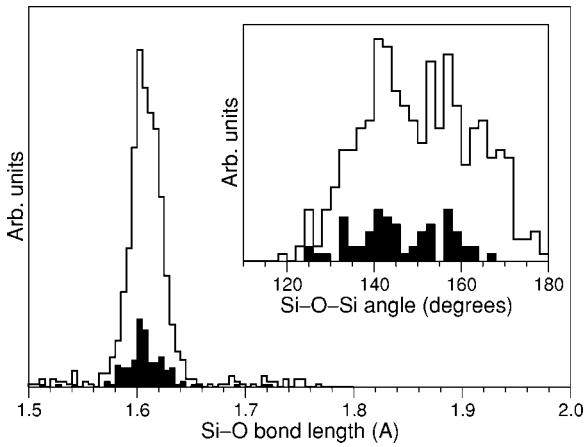

FIG. 1. Distributions of Si—O distances in a MD-simulated 648-atom a-SiO_2 structure. Inset shows the distribution of Si—O—Si angles in the same structure. Shaded areas show the distributions found for the subset of oxygen sites selected for the embedded cluster calculations.

was initially relaxed without the vacancy, as discussed in Refs. 29 and 35. Then the neutral vacancy was created by removing the central oxygen atom. The formation energies (E_{form}) were calculated with respect to the total energy of the corresponding nondefective QM cluster and free oxygen atom in the triplet state. We also analyzed the distribution of defect relaxation energies (E_{rel}) defined as the total energy difference between the fully relaxed and unrelaxed systems with the vacancy. This energy is taken as a measure of the defect-induced network distortion.

In all cases we find that the removal of an oxygen atom is accompanied by Si—Si bond formation. The distance between the two Si ions becomes much shorter than the original distance and as the Si ions move closer to each other they pull the network ions with them. However, the bond length and details of the lattice relaxation in the vicinity of the defect depend on the structure of local- and medium-range environments of the original site. These properties can be characterized in terms of distributions of structural and energetic parameters. For example, the distribution obtained for the oxygen vacancy formation energies is shown in Fig. 2. It has a full width at half maximum (FWHM) of about 1.8 eV with the maximum between 4.2 and 4.4 eV. The latter should be compared with the formation energy of 4.5 eV[21] for the oxygen vacancy in α-quartz calculated using a QM cluster of the same size. As discussed in earlier work,[21] the absolute value of the formation energy depends on the basis set and size of the QM cluster, but the shape and the width of the distribution should not depend significantly on these parameters.

To reveal the factors contributing to the distribution of formation energies, we first note (see Fig. 2) that the formation energies are much larger and their distribution is much narrower if no relaxation of the amorphous network is taken into account. This relatively narrow distribution reflects the site-to-site variation in the strength of the chemical bonds between the oxygen and its nearest Si neighbors. The real formation energies are much smaller due to the network re-

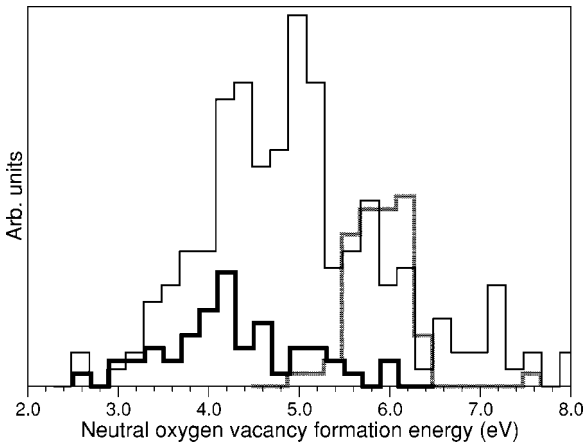

FIG. 2. Distributions of NOV formation energies (E_{from}). Gray and black thick lines show the distributions of E_{from} calculated using the embedded cluster approach for unrelaxed and relaxed oxygen vacancies, respectively. (The statistics were taken over 75 sites.) The thin line shows the distribution of relative E_{from} calculated using classical static calculations for relaxed oxygen vacancies. (The statistics were taken over 220 sites.)

laxation; the site-to-site variations of the relaxation energy reflect the difference between the local- and medium-range structures of different sites. The final vacancy formation energies can be represented as a sum of two contributions. The first one could be called a short-range contribution $\Delta E_{sr} = E_{sr}(ideal) - E_{sr}(Vac) - E(\mathrm{O})$, where E_{sr} is the energy of the QM cluster in the electrostatic potential of the rest of the system and $E(\mathrm{O})$ is the energy of the free oxygen atom in the triplet state. The second component ΔE_{mr} can be considered as a medium-range one, and includes the change in the interaction between the classical ions outside the QM cluster caused by their displacements and also by the distortion of the QM cluster. The short-range contribution is, on average, about three times larger than the medium-range one, but the widths of the distributions of both components are approximately the same with FWHM close to 1 eV (not shown). It is interesting to note the similarity of this result with the analysis of short- and medium-range contributions to the incorporation energy distribution of peroxy linkage in Refs. 5 and 44. However, in the latter case, the incorporation of an additional oxygen atom at the oxygen site led to the network relaxation occurring predominantly away from the defect.

A significant difference in the distributions of the unrelaxed and relaxed vacancy formation energies suggests that there could be some relation between the formation and relaxation energies of NOVs. Indeed, the data presented in Fig. 3 demonstrate a clear anticorrelation between them: large relaxation energy corresponds to small vacancy formation energy. This shows that the formation of vacancies at some oxygen sites in a-SiO_2 induces a large relaxation of the environment and that this relaxation favors the vacancy formation. The relaxation energies can vary significantly from site to site. For example, the smallest E_{rel} in Fig. 3 is just under 0.5 eV and the largest one is over 2.5 eV. These numbers can be compared with the 2.0 eV relaxation energy calculated using a similar technique for the NOV in α-quartz.

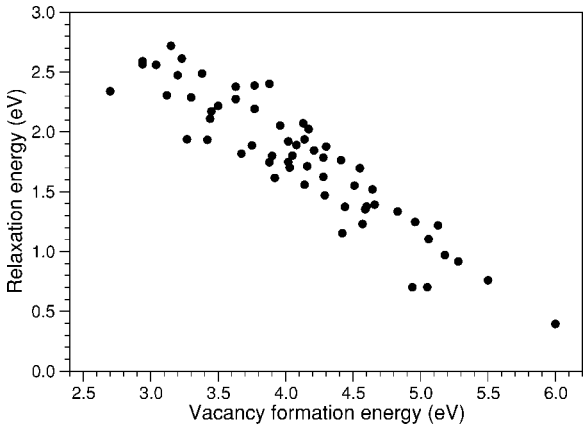

FIG. 3. Correlation between the vacancy formation energies (E_{from}) and the corresponding relaxation energies (E_{rel}) calculated for the oxygen vacancies at the 75 selected lattice sites.

To illustrate this point further, in Fig. 4 we have plotted the vacancy formation energies as a function of the Si—Si distance in the relaxed vacancy. We find that a large structural relaxation promotes formation of vacancies with small Si—Si distances and small vacancy formation energies. Further analysis demonstrates that the relaxation energy is strongly correlated with the displacements of these two Si atoms from their original sites in the nondefective amorphous structure.

Finally, the full extent of vacancy-induced network relaxation is illustrated in Fig. 5 where we present the projections of displacements of all the ions around one of the vacancies onto the vector connecting the original position of each ion and the vacancy site. One can see that the ion displacements near the vacancy are directed preferentially toward the vacancy and that the field of displacements propagates as far as 10 Å away from the vacancy site. At the same time, some of the atoms at distances larger than 3 Å from the vacancy site displace not toward the vacancy but away from it. The vacancy-induced relaxation also results in the deformation and effective rotation of SiO_4 tetrahedra nearest to the vacancy.

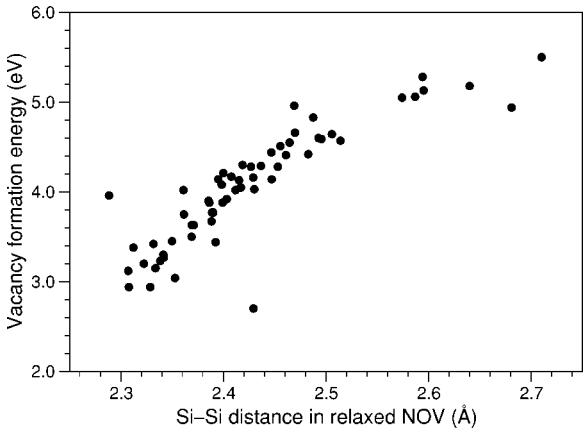

FIG. 4. Correlation between Si—Si distances in the neutral vacancies and vacancy formation energies calculated for the 75 selected lattice sites.

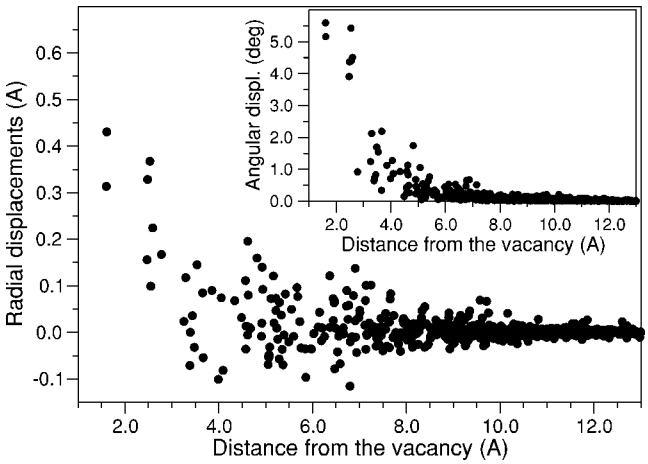

FIG. 5. Radial displacements of ions in the amorphous silica network induced by the formation of a neutral oxygen vacancy. Negative displacements correspond to displacements away from the vacancy. The inset shows the rotational displacements of the atoms around one of the vacancies from their nondefective positions. The character of these displacements is similar for all vacancies.

The formation of a neutral oxygen vacancy induces a doubly occupied energy level in the silica band gap. The position of this level with respect to the top of the valence band can be characterized using a parameter $\Delta\epsilon$ defined as the difference between the one-electron energies of the highest occupied state of the valence band (HOMO) and the vacancy state. The distribution of $\Delta\epsilon$ calculated for NOVs at 75 sites is shown in Fig. 6. The HOMO only approximately represents the position of the top of the valence band in the material as it is affected by the particular position of the NOV in the amorphous network and by the degree of the NOV-induced lattice distortion. Nevertheless, the broad distribution seen in Fig. 6 clearly demonstrates the extent of inhomogeneous broadening of defect levels in amorphous silica and could be relevant to the possible role of NOV in MOS devices.[1]

The wide spread of distances and defect energy levels indicates that, if all the configurations are realized with equal probability, there could be a wide distribution of optical excitation energies. Experimentally, the optical absorption spectra assigned to the neutral oxygen vacancies show a characteristic peak at 7.6 eV and, in some unirradiated samples, a tail in the 6.0–7.0 eV region.[17,19,24,25] These experimental and our theoretical results suggests that most of the NOV should contribute to the 7.6 eV peak and that the additional absorption in the red part of the spectrum could be due to vacancies with specific properties.

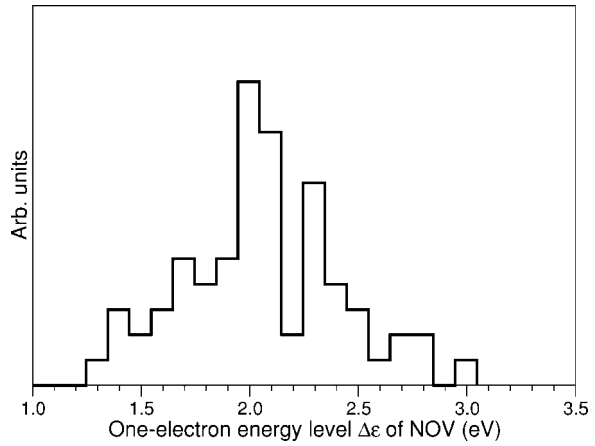

FIG. 6. Distribution of one-electron energies of occupied NOV-induced states with respect to the top of the valence band ($\Delta\epsilon$).

To check whether the ground state properties of NOVs are correlated with their optical absorption, we built a statistically more representative distribution of NOV properties as described in the next section. The optical absorption spectra calculated for a subset of NOVs are discussed in Sec. III C.

B. Classical simulations

To obtain a statistically more representative set of NOVs we used classical simulations. In these simulations the NOV was described using a set of classical interatomic potentials. The effective charge of the oxygen ion ($-1.2\,e$), which has been removed to create a vacancy, was equally distributed between the two Si atoms neighboring the vacant site, so these Si atoms have charges of $1.8\,e$ each. A neutral and massless species was placed at the original oxygen site and Buckingham-type pair potentials were derived to describe the interaction of this species with the neighboring Si and O ions. The parameters of these potentials were fitted to reproduce a set of defect configurations and their relative energies obtained using the embedded cluster method for NOVs in α-quartz and a-SiO_2. The parameters of the potentials defined between the two Si atoms near the vacancy and their oxygen neighbors and the parameters of the O—O potentials for these oxygens have also been modified. The interactions between all other lattice ions were unchanged.[29,31] Thus the vacancy was described by a pseudoatom interacting through pairwise potentials with its nearest neighbors. In static energy minimization calculations the position of this atom was optimized together with all other ions.

Using these potentials we carried out classical static calculations of NOV in 220 sites selected at random from the 648-atom amorphous structure introduced above. The distribution of relative values of vacancy formation energies is shown in Fig. 2. The formation energies obtained from classical calculations are much larger than those obtained from quantum-mechanical calculations. This is mainly due to the fact that the energy of a free atom is not defined in classical calculations. To compare the obtained distribution with the one obtained using the embedded cluster method, we shifted the classical formation energies by approximately 20 eV so that the low-energy tail of their distribution matched the low-energy tail of the E_{form} distribution calculated quantum-mechanically in the previous section.

As one can see in Fig. 2, the distribution obtained using classical simulations is wider than that obtained using the embedded cluster method for the set of 75 sites. This could be partly due to the larger sample and partly due to deficiencies in the classical description of NOV, which is unable to reproduce the details of the electron density distribution for "short" and "long" Si—Si bonds. We should note that there

is no complete one-to-one correlation between the relative formation energies found using classical and QM calculations in the same sites. Although the order of some configurations changes, statistically, they belong to the same parts of the distributions in Fig. 2.

Maxima in both distributions correspond to the "most probable" sites for forming a NOV in our amorphous sample. These are, however, not the sites that are most likely to host a vacancy under thermal equilibrium conditions. For both the classical and QM distributions from randomly selected vacancies, the low-energy tail of the formation energy distribution represents the minority of species. On the contrary, in the thermal equilibrium, most of the vacancies are expected to occupy sites with low formation energies. Although the span of the "low" formation energies is likely to be similar in both cases, the corresponding distributions may differ.

To test this assertion, we carried out high temperature annealing of our defect structures using classical MD. For that purpose we selected 20 vacancy configurations from the low-energy tail ($E_{from} < 4.0$ eV) of the classical formation energy distribution. In addition, three vacancy configurations with $E_{from} > 4.5$ eV were included in the same set. The Si—Si distances at neutral vacancies were below 2.4 Å for the first group and above 2.5 Å for the second group. As noted above, the classical and embedded cluster calculations are consistent in predicting that the selected 20 vacancies are at the low-energy tail of the formation energy distribution. Therefore in a further discussion we use the QM formation energy scale for both classical and QM calculations.

To anneal the vacancies, we used the same 648-atom supercell and the same parametrization for the vacancy interactions as in the classical static energy minimization calculations described above. The calculations were carried out using the DL_POLY code[30] and an NVT ensemble. Starting with the fully relaxed vacancy configuration, the system was heated up to 1000 K at a rate of 6 ps per 100 K at constant volume. After heating, the system was equilibrated at 1000 K for another 20 ps and then cooled to 0 K at 6 ps per 100 K rate. We observed that above 1000 K the Si—Si bond is about to break for some vacancy sites so the temperature was never increased above that. Finally, the system was equilibrated at 0 K and at constant pressure for another 20 ps and then fully relaxed using static energy minimization.

We found that at those sites where vacancy formation energy was already low in the static relaxation, the MD-annealing did not change the formation energy by more than 5 meV and the corresponding Si—Si distance after annealing changed by less than 0.01 Å. The maximum change in the Si—O—Si angles for these sites is close to 10°. However, for the three sites, out of the selected set of 23, where static relaxation energies were small and the corresponding vacancy formation energies were larger than 4.5 eV (4.6, 4.7, and 5.6 eV), the MD annealing helped to relax the structure further and resulted in lower-energy vacancy configurations with the formation energies reduced by 0.85, 0.9, and 1.1 eV, respectively. The corresponding Si—Si distances decreased by 0.09, 0.07, and 0.1 Å, while the change in the lattice Si—O—Si angles was about 20°.

These preliminary results demonstrate that a high temperature anneal can lead to a different (perhaps more narrow) distribution of vacancy formation energies than that obtained using the static calculations. Further work is in progress to elucidate this issue. Since the low formation energy defects remained largely unaffected by the anneal, in this work we will use the vacancies at the low-energy tail of the *random* distribution to model the properties of the vacancies at the *thermal equilibrium*.

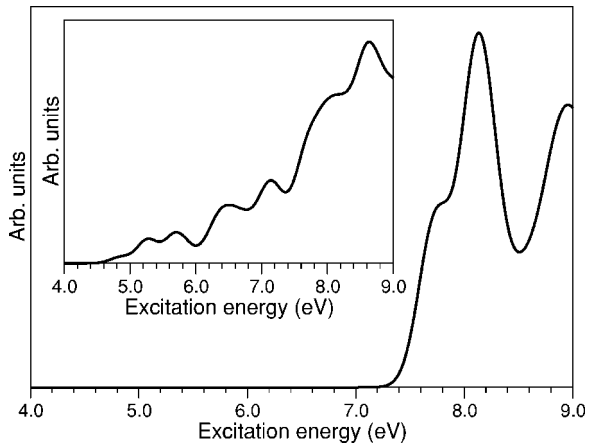

FIG. 7. Optical absorption spectra calculated for 23 neutral vacancy configurations at different lattice sites. Each individual spectrum was weighed with the Boltzmann factor and corresponding vacancy formation energy. Inset shows the original (not weighed) absorption spectra for the same selection of 23 vacancies.

C. Calculation of optical absorption spectra

The optical absorption spectra were calculated for the same set of 23 vacancies as described above in Sec. III B. Each vacancy was fully relaxed using the embedded cluster method and then the 25 lowest energy transitions were calculated for each of them. $Si_2O_7Si_6^*$ QM clusters were used in most calculations. The ground state calculations were made using DFT with a modified B3LYP density functional with 32.5% of exact exchange.[43] The optical excitation energies were calculated using the time-dependent DFT method as implemented in the GAUSSIAN98 code.[42]

The optical absorption spectrum shown in Fig. 7 was obtained by summing up the individual spectra obtained for each of the 23 sites. The envelope curve is produced by broadening each transition with excitation energy E_i by a Gaussian-type function $f_i(E) = e^{-(E-E_i)^2/2\sigma^2}$ with the σ parameter equal to 0.15 eV. The spectrum obtained is shown in the inset in Fig. 7; it shows a maximum at approximately 8.5 eV and a prominent tail that reaches to 5 eV in the red part of the spectrum.

The low energy part of the spectrum is mainly determined by the transition between the bonding σ and antibonding σ^* states of the NOV. Both states are located in the band gap and contribute to the optical transitions up to 7.8 eV. The splitting between the one-electron energies of σ and σ^* states is generally smaller for the vacancies with longer Si—Si bonds. Consequently, the energies of the bonding (σ)-antibonding (σ^*) transitions for these vacancies are much lower than those for short Si—Si bonds. At the same

time, longer Si—Si bonds correspond, statistically, to the vacancies with larger formation energies (see Fig. 4). Thus the low-energy tail of the optical absorption should be mostly determined by the vacancies that have larger formation energies.

At higher energies, the optical absorption is dominated by transitions between the σ and π states of the vacancies and transitions between the valence band states and σ^* and π states of the vacancies. The oscillator strength of these transitions is typically several times lower than that for the main bonding σ to antibonding σ^* transitions. A further contribution to the absorption spectrum comes from band-to-band transitions. The transitions of this type included in the first 25 excited states contribute to the peak at approximately 8.5 eV (inset in Fig. 7).

To take into account only the most populated vacancy configurations at thermal equilibrium, the optical absorption spectrum was then weighted with the Boltzmann factor $e^{-E_{form}/kT}$, where E_{form} is the vacancy formation energy calculated using the B3LYP functional, k is the Boltzmann constant, and T is temperature. The spectrum shown in Fig. 7 was calculated for $T=300$ K.

After this adjustment the shape of the absorption spectrum has changed considerably: the tail between 5 and 7 eV has disappeared and the maximum at 8.5 eV has shifted to 8.1 eV. Due to their large formation energies the long bonded Si—Si configurations included in the selection of 23 NOV sites do not contribute to the weighted optical absorption spectrum at room temperature. Therefore the tail reflects the presence of the vacancies with Si—Si bond lengths exceeding the one found for vacancies with the lowest formation energy, i.e., around 2.3 Å. Thus the optical absorption in the energy range of 6 to 7 eV reported, for example, in Ref. 25 could reflect the distribution of the Si—Si distances in a particular sample.

To check the dependence of this conclusion on the QM cluster size we selected two NOV configurations out of 23 and calculated their ground state properties and the optical absorption spectra using larger QM clusters $Si_8O_{25}Si^*_{18}$ and $Si_9O_{27}Si^*_{18}$ and the same 6-31G basis set. The results obtained is these calculations are consistent with those obtained from using small clusters. In particular, they confirmed that the vacancy with the larger formation energy has a longer Si—Si bond and a lower energy of the $\sigma \rightarrow \sigma^*$ transition. However, the relative intensities of individual electronic transitions depend significantly on the cluster size.

This is primarily due to two factors. First, the smaller QM clusters impose artificial constraints on the character of localization of the defect-induced occupied and unoccupied states. As a result, the kinetic energy of these states is overestimated and, hence, the calculated energies of the defect optical absorption are shifted to the higher energies. The effect is smaller for genuinely localized defect states. In the case of the neutral oxygen vacancies the energies of the $\sigma \rightarrow \sigma^*$ transitions calculated using large clusters are typically 0.3 eV smaller than those calculated using small clusters. Second, the valence band (VB) and the conduction band (CB) states are more delocalized in the case of large clusters. Consequently, the oscillator strength of the optical transitions that involve VB and CB states are smaller and the contributions of these transitions to the optical absorption spectra are less prominent. The latter is, of course, counterbalanced by the fact that there are more VB and CB states in the large clusters than in the small ones.

IV. DISCUSSION AND CONCLUSIONS

We have characterized neutral oxygen vacancies in amorphous silica using both quantum-mechanical embedded cluster and classical calculations. In particular, we have calculated the distributions of the vacancy formation energies and correlated these energies with other properties of the vacancies including their geometrical parameters (Si—Si distances) and optical absorption.

The two formation energies distributions obtained for 75 and 220 sites are likely to correctly reflect the structural properties of our a-SiO_2 sample. They give an estimate of which oxygen sites will be occupied by vacancies at thermal equilibrium. This distribution may change if all of the vacancy configurations are annealed using molecular dynamics. Consequently, distributions of other properties, when weighted with a Boltzmann factor $e^{-E_{form}/kT}$ will change too. A more accurate distribution of the formation energies can be obtained if QM molecular dynamics is used to model the annealing process. At the same time, our preliminary results indicate that the properties of the vacancies at the low-energy tail of the formation energies are not strongly affected by the molecular dynamics anneal. Therefore such vacancies could be used to model the most probable NOV configurations.

Our results suggest that larger formation energies correspond, statistically, to vacancies with longer Si—Si bonds. These result in a smaller splitting between the one-electron energies of vacancy-induced σ and σ^* states and, consequently, to lower $\sigma \rightarrow \sigma^*$ transition energies. Thus the red tail of the NOV optical absorption is determined by the relative concentration of the vacancies with longer Si—Si bonds. Since such vacancies have larger formation energies, the red part of the NOV optical absorption spectrum should strongly depend on the details of sample preparation and any further treatment which can create NOV. We have also calculated the distribution of the one-electron energies of the vacancy states with respect to the top of the valence band. These results demonstrate that there is a significant proportion of vacancy sites where the occupied σ state is as high as 2.5–3 eV above the VB top. These vacancies may affect the performance of nanosized MOS devices.

The classical calculations also allow us to estimate the NOV-induced volume change.[45,46] This is done by optimizing both the fractional coordinates and the unit cell parameters of the 648-atom structure for each particular configuration of NOV. The concentration of vacancies in our calculations corresponds to 1.1×10^{20} vacancies per cm^3. We found that most of the vacancies cause the volume of the unit cell to decrease between 0 and 0.5% with only a small number of cases of expansion (see the distribution of the volume change shown in Fig. 8). On the other hand, if, as a result of the vacancy formation, an oxygen atom is removed from the system altogether, the total mass of the 648-atom supercell is decreased by 0.12%. Since the change in the volume is more

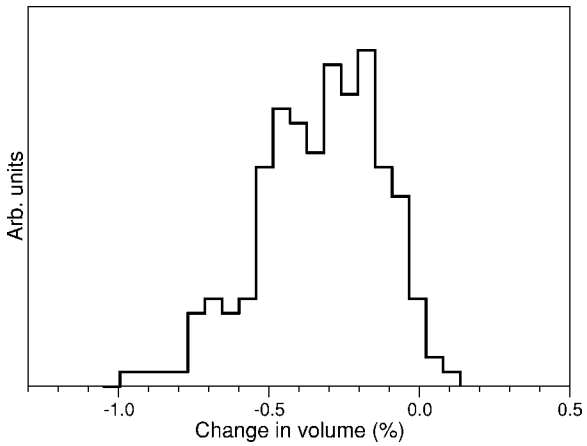

FIG. 8. Distribution of the volume change per supercell induced by the neutral oxygen vacancy formation.

substantial than the change in mass, one can conclude that on average formation of NOV should lead to densification of silica samples.

To summarize, we applied a statistical approach to study the distribution of structural and optical properties of neutral oxygen vacancies in amorphous silica using the embedded cluster method. This approach allows one: (i) to study the full extent of the defect-induced lattice distortion; (ii) to consider a fairly large region of the amorphous structure and thus to explore a greater variety of different sites in the amorphous structure and to build more complete statistics of different defect types and configurations; and (iii) to calculate a wide range of defect properties, including the optical absorption spectra. The experience gained in these calculations and in combining quantum mechanical and classical techniques will be useful for further studies of defects in disordered materials.

ACKNOWLEDGMENTS

The authors would like to thank K. Tanimura, A. H. Edwards, D. L. Griscom, L. Skuja, A. Trukhin, V. Mashkov, H. Hosono, M. Hirano, K. Kajihara, and C. Bird for useful discussions. We are grateful to A. S. Mysovsky and A. Taga for their contributions in developing an embedding potential for SiO_2. The work is supported by EPSRC, EU Framework5 project HIKE, JST and by the Grant-in-Aid for Creative Scientific Research No. 16GS0205 from the Japanese Ministry of Education, Culture, Sports, Science and Technology. The computer time on the HPCx facility was awarded to the Materials Chemistry consortium under EPSRC Grant GR/S13422/01 "Materials Chemistry using Tera-scale Computing."

*Corresponding author. Email address: s.mukhopadhyay@ucl.ac.uk
†Corresponding author. Email address: a.shluger@ucl.ac.uk

[1] *Defects in* SiO_2 *and Related Dielectrics: Science and Technology*, *NATO Science Series, Series II: Mathematical and Physical Chemistry*, edited by G. Pacchioni, L. Skuja, and D. L. Griscom (Kluwer Academic Publishers, Dordrecht, 2000).
[2] *Structure and Imperfections in Amorphous and Crystalline Silicon Dioxide*, edited by R. A. B. Devine, J.-P. Duraud, and E. Dooryhée (Wiley, New York, 2000).
[3] A. L. Shluger, A. S. Foster, J. L. Gavartin, and P. V. Sushko, in *Nano and Giga Challenges in Microelectronics*, edited by J. Greer, A. Korkin, and J. Labanowski (Elsevier, New York, 2003), pp. 151–222.
[4] E. A. Kotomin and A. I. Popov, Nucl. Instrum. Methods Phys. Res. B **141**, 1 (1998).
[5] M. A. Szymanski, A. L. Shluger, and A. M. Stoneham, Phys. Rev. B **63**, 224207 (2001).
[6] D. Donadio, M. Bernasconi, and M. Boero, Phys. Rev. Lett. **87**, 195504 (2001).
[7] A. Bongiorno and A. Pasquarello, Phys. Rev. Lett. **88**, 125901 (2002).
[8] Z.-Y. Lu, C. J. Nicklaw, D. M. Fleetwood, R. D. Schrimpf, and S. T. Pantelides, Phys. Rev. Lett. **89**, 285505 (2002).
[9] D. L. Griscom, in *Defects in* SiO_2 *and Related Dielectrics: Science and Technology*, *NATO Science Series, Series II: Mathematical and Physical Chemistry*, edited by G. Pacchioni, L. Skuja, and D. L. Griscom (Kluwer Academic Publishers, Dordrecht, 2000), pp. 117–160.
[10] P. M. Lenahan and J. J. F. Conley, J. Vac. Sci. Technol. B **16**, 2134 (1998).
[11] A. Stesmans, B. Nouwen, and V. V. Afanas'ev, Phys. Rev. B **66**, 045307 (2002).
[12] A. Othonos and K. Kalli, *Fiber Bragg Gratings Fundamentals and Applications in Telecommunications and Sensing* (Artech House, Boston, 1999).
[13] D. L. Griscom and M. Cook, J. Non-Cryst. Solids **182**, 119 (1995).
[14] L. Skuja, J. Non-Cryst. Solids **239**, 16 (1998).
[15] S. Agnello, R. Boscaino, G. Buscarino, M. Cannas, and F. M. Gelardi, Phys. Rev. B **66**, 113201 (2002).
[16] S. Agnello, R. Boscaino, F. M. Gelardi, and B. Boizot, J. Appl. Phys. **89**, 6002 (2001).
[17] M. Guzzi, F. Pio, G. Spinolo, A. Vedda, C. B. Azzoni, and A. Paleari, J. Phys.: Condens. Matter **4**, 8635 (1992).
[18] M. K. Schurman and M. Tomozawa, J. Non-Cryst. Solids **202**, 93 (1996).
[19] A. N. Trukhin and H. J. Fitting, J. Non-Cryst. Solids **248**, 49 (1999).
[20] G. Pacchioni, G. Ieranò, and A. M. Márquez, Phys. Rev. Lett. **81**, 377 (1998).
[21] V. B. Sulimov, P. V. Sushko, A. H. Edwards, A. L. Shluger, and A. M. Stoneham, Phys. Rev. B **66**, 024108 (2002).
[22] T. Tamura, G. H. Lu, R. Yamamoto, and M. Kohyama, Phys. Rev. B **69**, 195204 (2004).
[23] G. Hetherinton, K. H. Jack, and M. W. Ramsay, Phys. Chem. Glasses **6**, 6 (1965).
[24] M. Cannas, F. M. Gelardi, A. C. F. Pullara, M. Barbera, and S. Varisco, J. Non-Cryst. Solids **280**, 188 (2001).

[25] A. Anedda, C. M. Caronara, R. Corpino, and A. Serpi, J. Non-Cryst. Solids **245**, 183 (1999).
[26] P. V. Sushko, A. L. Shluger, and C. R. A. Catlow, Surf. Sci. **450**, 153 (2000).
[27] A. S. Mysovsky, P. V. Sushko, S. Mukhopadhyay, A. H. Edwards, and A. L. Shluger, Phys. Rev. B **69**, 085202 (2004).
[28] K. Vollmayr, W. Kob, and K. Binder, Phys. Rev. B **54**, 15808 (1996).
[29] S. Mukhopadhyay, P. V. Sushko, A. M. Stoneham, and A. L. Shluger, Phys. Rev. B **70**, 195203 (2004).
[30] W. Smith and T. R. Forester, J. Mol. Graphics **14**, 136 (1996).
[31] B. W. H. van Beest, G. J. Kramer, and R. A. van Santen, Phys. Rev. Lett. **64**, 1955 (1990).
[32] A. Navrotsky, Diffus. Defect Data **53/54**, 61 (1987).
[33] J. D. Gale and A. L. Rohl, Mol. Simul. **29**, 291 (2003).
[34] B. G. Dick and A. W. Overhauser, Phys. Rev. **112**, 90 (1958).
[35] S. Mukhopadhyay, P. V. Sushko, A. H. Edwards, and A. L. Shluger, J. Non-Cryst. Solids **345** & **346**, 703 (2004).
[36] J. S. Braithwaite, P. V. Sushko, K. Wright, and C. R. A. Catlow, J. Chem. Phys. **116**, 2628 (2002).
[37] P. V. Sushko, A. L. Shluger, K. Hayashi, M. Hirano, and H. Hosono, Phys. Rev. Lett. **91**, 126401 (2003).
[38] V. A. Nasluzov, E. A. Ivanova, A. M. Shor, G. N. Vayssilov, U. Birkenheuer, and N. Rösch, J. Phys. Chem. B **107**, 2228 (2003).
[39] P. Sherwood, A. H. de Vries, M. F. Guest, G. Schreckenbach, C. R. A. Catlow, S. A. French, A. A. Sokol, S. T. Bromley, W. Thiel, A. J. Turner *et al.*, J. Phys.: Condens. Matter **632**, 1 (2003).
[40] D. Erbetta, D. Ricci, and G. Pacchioni, J. Chem. Phys. **113**, 10744 (2000).
[41] T. Uchino, M. Takahashi, and T. Yoko, Phys. Rev. Lett. **86**, 5522 (2001).
[42] M. J. Frisch, G. W. Trucks, H. B. Schlegel, G. E. Scuseria, M. A. Robb, J. R. Cheeseman, V. G. Zakrzewski, J. J. A. Montgomery, R. E. Stratmann, J. C. Burant *et al.*, *GAUSSIAN 98 (Revision A.7)*, Gaussian Inc., Pittsburgh, PA, 1998.
[43] A. V. Taga, P. V. Sushko, and A. L. Shluger (unpublished).
[44] D. Ricci, G. Pacchioni, M. A. Szymanski, A. L. Shluger, and A. M. Stoneham, Phys. Rev. B **64**, 224104 (2001).
[45] A. M. Stoneham, J. Phys. C **16**, L925 (1983).
[46] Y. Ikuta, K. Kajihara, M. Hirano, and H. Hosono, Appl. Opt. **43**, 2332 (2004).